Shear-compression tests of URM walls: various setups and their influence on experimental results

Bastian Valentin Wilding[1]

bastian.wilding@epfl.ch

Kiarash M. Dolatshahi[1,2]

dolatshahi@sharif.edu

Katrin Beyer[1] – corresponding author

katrin.beyer@epfl.ch

[1]Earthquake Engineering and Structural Dynamics Laboratory (EESD), School of Architecture, Civil and Environmental Engineering (ENAC), École Polytechnique Fédérale de Lausanne (EPFL), EPFL ENAC IIC EESD, GC B2 504, Station 18, 1015 Lausanne, Switzerland

[2]Department of Civil Engineering, Sharif University of Technology, Room 515, Tehran, Iran

Abstract

Current design codes provide empirical equations for the drift capacity of unreinforced masonry (URM) walls that are based on results of quasi-static cyclic shear-compression tests. Yet different experimental campaigns have used various approaches of imposing fixed-fixed boundary conditions at the wall top which may affect the test results. This article investigates, by means of numerical simulations, the influence of experimental setups on the force and drift capacities of in-plane loaded URM walls subjected to double-fixed conditions. It is shown that controlling the shear span or the top rotation while keeping the axial force constant leads to very similar results. Controlling the axial elongation at the top of the wall results for walls subjected to a small axial load ratio in an increase and for walls subjected to a large axial load ratio in a decrease in axial load with increasing drift demands. Testing half the wall applying cantilever boundary conditions is not recommended as the stiff loading beam at the wall top changes the failure mode and leads to significantly larger drift capacities.

Keywords: *unreinforced masonry wall, quasi-static cyclic test, drift capacity, kinematic boundary conditions, changing axial load, non-linear numerical simulation*

1 Introduction

Shear-compression tests are typically used to characterise the force and drift capacity of in-plane loaded unreinforced masonry (URM) walls. In these tests, the masonry walls are subjected to horizontal in-plane displacements while being loaded vertically at the same time (e.g. [1–10]). When conducting such a test, two decisions regarding the three in-plane degrees of freedom at the wall top need to be taken.

The first concerns the horizontal displacement, which can be applied monotonically increasing or—which is more common—as a sequence of horizontal displacement cycles. In case of the latter, the sequence of horizontal cycles, the loading protocol needs to be chosen. There is little experimental evidence with regard to the influence of the loading protocol on the obtained force and drift capacities. Only two campaigns tested pairs of walls under cyclic and monotonic loading [1,2], which showed that the loading protocol had a relatively small influence on the force but a strong effect on the drift capacities [11]. A recently conducted numerical study on the influence of loading protocols supports this evidence and investigates furthermore the effects a change in cycle number, cycle mean and the order of cycles can have on the wall behaviour [12].

The second decision is about the control of the axial force and the in-plane moment at the wall top or their corresponding displacement quantities (axial displacement, in-plane top rotation). It is of equal importance, since it is well established that an increase in axial force or a decrease in shear span leads to an increase in force capacity and a reduction in drift capacity (e.g. [11]). Commonly, either cantilever or double-fixed boundary conditions are simulated in shear-compression tests. While there is little ambiguity with regard to the setup for cantilever tests, various test configurations have been used to impose fixed-fixed boundary conditions at the wall top. Four different setups can be distinguished, each of which might lead to differences in terms of strength and displacement capacities. Yet when deriving empirical drift capacity models, e.g. [6,11], the possible influence of the different test setups is not accounted for, which might partly explain the variability typically associated with drift capacity models.

This article investigates the influence of the different test setups for simulating double-fixed boundary conditions on the URM wall behaviour by means of numerical simulations of cyclic shear-compression tests. The numerical simulations are conducted using a meso-scale modelling approach [13] and the chosen kinematic and static boundary conditions represent commonly used test setups imposing double-fixed

boundary conditions. The various used test setups for simulating double-fixed conditions are introduced in Sect. 2. The numerical modelling approach with its main assumptions and characteristics is presented in Sect. 3. In Sect. 4, the results are presented, the influence of the boundary conditions on the wall behaviour discussed and in Sect. 5 conclusions are drawn.

2 Boundary conditions in test setups for shear-compression tests

To the authors' knowledge, four ways of applying fixed-fixed boundary conditions in in-plane shear-compression tests of URM walls have been used in the past, which differ with regard to the control of the degrees of freedom at the top of the wall. At the base, the walls are always supported by a stiff foundation. All test setups include a rigid loading beam that is placed on top of the test unit and therefore the in-plane degrees of freedom at the wall top reduce to three. The chosen cyclic loading protocol (e.g. [14]) determines the horizontal top displacement; the horizontal actuator is therefore always operated in a displacement-controlled mode. For the two other degrees of freedom, either the static (axial force N, top moment M) or the equivalent kinematic quantity (axial elongation w, top rotation θ) can be controlled. Four combinations have been used in various test campaigns, which are described in the following sections.

2.1 Force control of vertical actuators

The approach of keeping the shear span (H_0) at half the wall height has been used recently by e.g. Magenes et al. [5] and Petry & Beyer [15]. The moment on the wall top is altered with two vertical actuators such that top and base moments are equal whilst keeping the total normal force $N = N_1 + N_2$ on the wall constant (Figure 1a). Petry & Beyer did not report any problems but Magenes et al. switched to a mixed control (Section 2.2) after having experiencing difficulties in controlling the actuators, which led to a brittle failure due to diagonal cracking of the first specimen. An advantage of the force-controlled approach for the vertical actuators is that any given shear span can be simulated as opposed to mixed control, which is essentially limited to simulating a shear span of half the wall height. Petry & Beyer [7] used the force-controlled mode to test walls with shear spans of $0.75H$ as well as $1.5H$. A photo of the used test setup is shown in Figure 2.

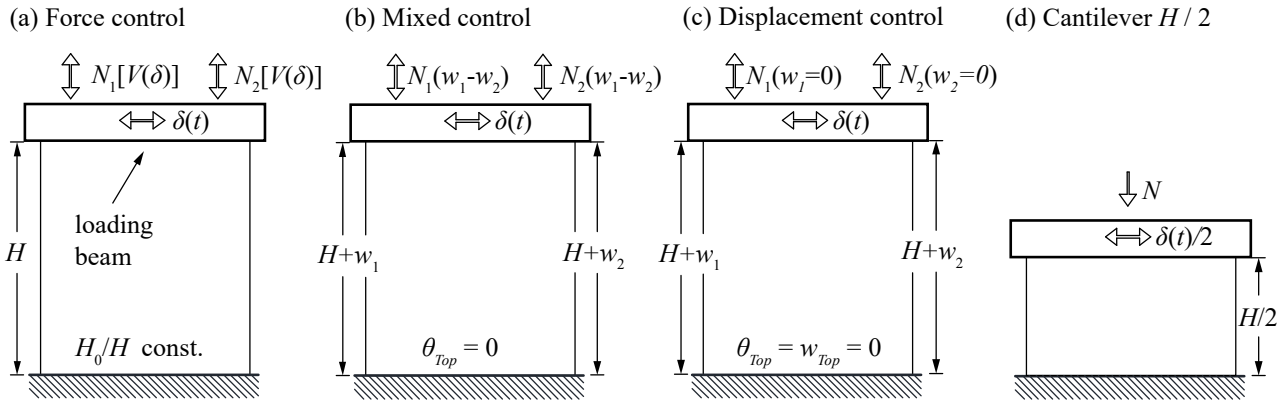

Figure 1: Different approaches to obtain fixed-fixed conditions in testing, (a) force control, (b) mixed control, (c) displacement control, (d) cantilever of half the wall height

Figure 2: Photo of the test setup by [7] with the two vertical actuators and the horizontal one

2.2 Mixed control of vertical actuators

Mixed control of the vertical actuators is characterized by imposing an equal vertical displacement at both wall ends ($w_1 = w_2$) resulting in zero rotation of the wall top (θ_{top}=0), while keeping the total normal force constant, see Figure 1b. These boundary conditions can be applied either by two servo-hydraulic controlled actuators

(e.g. [5–7,10]) or by one actuator and mechanical devices (parallelograms) that restrain the top rotation (e.g. [16]). Salmanpour and Mojsilovic suggest that this way of testing is preferable to the force-controlled mode since they consider the boundary conditions to be more realistic [6,17].

2.3 Displacement control of vertical actuators

This kinematic boundary condition can be achieved by inserting rollers in-between loading beam and upper support or by means of two actuators on top restraining a change in wall height and top rotation (Figure 1c). Typically the normal force is applied before the axial displacement is restrained. As a consequence of restraining the axial degree of freedom, the axial force in the wall changes as soon as the wall cracks due to horizontal loading. This approach was used for example by Magenes & Calvi [2].

2.4 Cantilever of half the wall height

The method of testing a wall as a cantilever in order to simulate a fixed-fixed wall twice the height has been applied in the past because the test setup is considerably simpler (Figure 1d). Yet the loading beam on the wall top, corresponding to mid-height of walls tested according to the other control-modes, confines the wall preventing the formation of crossing diagonal cracks which are a typical failure mode under fixed-fixed boundary conditions. For this reason, the test setup is, to the authors' knowledge, no longer used.

3 **Analysis procedure**

The influence of the various presented test setups on the wall response is studied through numerical simulations of cyclic shear-compression tests of in-plane loaded URM walls in Abaqus/Explicit [18]. In the following, the analysis procedure is introduced.

3.1 Finite element model

The URM walls are modelled using the meso-scale modelling approach and a material subroutine by Aref and Dolatshahi [13], which is based on the works by Lourenço [19] and Oliveira et al. [20]. The brick units are expanded on each side by half the mortar joint width and modelled as solid elements (C3D8R). Interface elements (COH3D8) are placed between the brick units representing the bed- and head-joints and vertically in

the middle of each brick representing a possible fracture plane through the unit.

3.1.1 Solid elements

The already in Abaqus 6.14 [18] available 'Concrete Damaged Plasticity' model is assigned to the solid elements (with the dimensionless parameters in the description of the 'Concrete Damaged Plasticity' model corresponding to the proposed default values for concrete [18]) and they are meshed with prisms of l_{mesh} = 7.5 cm, h_{mesh} = 10.1 cm and t_{mesh} = 7.5 cm. As for the required uni-axial laws in compression and tension; the elastic modulus is determined based on the brick compressive strength ($E_b = 400\, f_{B,c}$), the used compressive uni-axial stress-strain law follows a suggestion by Kaushik et al. [21] and the uni-axial response in tension is determined by a linear-elastic pre- and an exponential post-peak response, which follows the formulation $\sigma_{in} = f_{B,t} \exp(- \varepsilon_{in}\, 10^3)$. The brick compressive strength $f_{B,c}$ and the masonry compressive strength f_u had been obtained in material tests of the experimental campaign [6] on which the simulated walls are based. The brick tensile strength $f_{B,t}$ was not determined in [6] and therefore taken from another campaign [7] since the same masonry typology was used. The parameters used in the 'Concrete Damaged Plasticity' model are summarized in Table 1.

Table 1: Parameters used for the material description of the solid elements in the 'Concrete Damaged Plasticity' model

E_b [MPa]	f_u [MPa]	$f_{B,t}$ [MPa]	ν [-]	ψ [deg]	ε [-]	σ_{b0}/σ_{c0} [-]	K_c [-]	μ [-]
10'520	5.86	1.27	0.15	31	0.1	1.16	2/3	0

E_b: elastic modulus brick, f_u: compressive strength masonry, $f_{B,t}$: tensile strength brick, ν: Poisson's ratio, ψ: dilation angle for flow potential equation, ε: eccentricity, parameter in flow potential equation, σ_{b0}/σ_{c0}: ratio of initial equibiaxial compressive yield stress to initial uniaxial compressive yield stress, K_c: constant in function describing yield surface, μ: viscosity parameter representing relaxation time of viscoplastic system in viscoplastic strain rate tensor

3.1.2 Interface elements

The behaviour of the interface elements is described by a VUMAT subroutine by Aref and Dolatshahi [13], which defines a plasticity model with a yield surface in shear and tension. The yield surface consists of a Mohr-Coulomb friction law with friction coefficient tan Φ and cohesion c and a straight tension cut-off at the tensile strength f_t. The degradation rate of said yield surface is governed by the fracture energies in tension (G_f^I) and shear (G_f^{II}). The cyclic reduction of the elastic normal (k_n) and shear ($k_{sx,y}$) stiffness of the interface elements is governed by the plastic multipliers and a degradation parameter (κ_1/κ_t) [22]. The normal stiffness k_n only reduces in tension; upon re-loading in compression it is set to its initial value for the simulation of opening and

closing of horizontal flexural cracks in bed-joints [13]. The reduction in shear stiffness $k_{sx,y}$ is limited to 20 % of the initial value, which appears to accurately capture the stiffness of the final cycles of the shear force-drift hysteresis. The used material parameters (whose origin is shown in [12]) are listed in Table 2.

Table 2: Material parameters used for the cohesive elements [12]

Parameter	Units	Hor. joint	Vert. joint	Mid. joint
f_t	[MPa]	0.14	0.04	1.27
G_f^I	[J/m²]	125	34	107
c	[MPa]	0.26	0.07	1.91
tan Φ	[-]	0.94	0.94	0.75
G_f^{II}	[J/m²]	1250	339	1068
k_n	[N/mm³]	28.9	7.81	400
$k_{sx,y}$	[N/mm³]	5.93	1.62	400
κ_1/κ_t	[-]	0.76	0.76	0.76

f_t: tensile strength, G_f^I: fracture energy Mode I, c: cohesion, tan Φ: friction coefficient, G_f^{II}: fracture energy Mode II, k_n: normal interface stiffness, $k_{sx,y}$: tangential interface stiffness, κ_1/κ_t: stiffness degradation parameter

3.2 Validation and analysed walls

The numerical modelling procedure has already been validated in [12,13,23] with tests from three different campaigns and has been shown to predict stiffness, force capacity and drift capacity in a reliable manner. Additionally, the comparison of shear-force drift curves between experimental results [6] of walls that correspond to the ones used in the following parametric study and the numerical model are shown in Figure 3 (their corresponding parameters are listed in Table 3). The walls were tested using the mixed-controlled mode for the vertical actuators and are simulated accordingly for the purpose of validation. The force-displacement behaviour seems to be well captured both in terms of force- and drift capacity along with stiffness degradation.

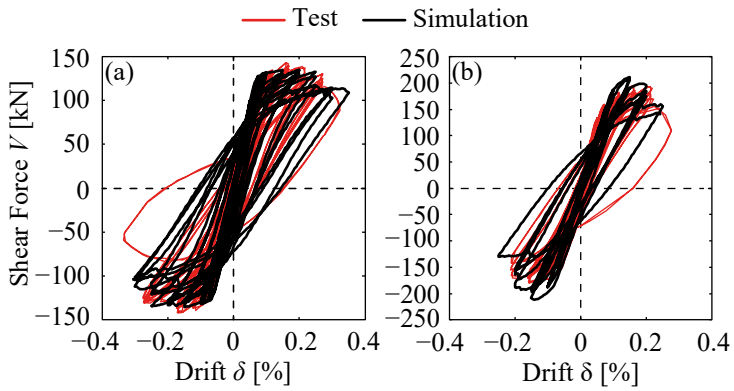

Figure 3: Shear force-drift curves of tests and numerical analysis, wall (a) T1 tested by [6], (b) T3 tested by [6]

In the parametric study (Sect. 4) four walls are analysed, which differ with regard to shear span and axial load

ratio. All the wall models simulated masonry panels made of perforated clay units with bed-joints of normal thickness and normal strength mortar. Their parameters correspond to tested walls by [6] as well as walls of half the length in order to investigate the behaviour of a larger range of walls. All analysed configurations are summarised in Table 3.

Table 3: Wall configurations analysed in Section 4

Name	L [mm]	H [mm]	T [mm]	l_B [mm]	h_B [mm]	σ_0 [MPa]	f_u [MPa]	$f_{B,c}$ [MPa]	σ_0 / f_u [%]
T1 [6]	2700	2600	150	290	190	0.58	5.80	26.3	10
T1 mod	1350	2600	150	290	190	0.58	5.80	26.3	10
T3 [6]	2700	2600	150	290	190	1.16	5.80	26.3	20
T3 mod	1350	2600	150	290	190	1.16	5.80	26.3	20

L: wall length, H: wall height, T: wall thickness, l_b: brick length, h_b: brick height, σ_0: axial stress applied at the beginning of the test, f_u: compressive strength of masonry, $f_{B,c}$: compressive strength of brick, σ_0/f_u: axial load ratio

3.3 Application of kinematic and static boundary conditions

The four different test setups for fixed-fixed boundary conditions are modelled as follows in Abaqus 6.14 [18] (Figure 4): In all models, the loading beam on top of the wall is simulated by a rigid plate (shell planar) connected to the wall with a surface-to-surface tie and the horizontal displacement history $v(t)$ is applied at a reference point representing a point mass, which is linked to the rigid plate.

- Force control of vertical actuators (N=const. & H_0=const.): to keep the shear span (H_0) at the required height during the simulation, the reference point is set at the shear span height. The horizontal displacement history ($v(t)$) is applied at the reference point (see Figure 4a), which does not belong to the masonry wall, while the normal force N is directly applied as four point loads at the corner points of the rigid plate.
- Mixed control of vertical actuators (N=const. & θ_{top}=0): to set the top rotation to zero, a rotational restraint is applied to the rigid plate on the wall top (Figure 4b). The normal force N is again applied as in the previous approach.
- Displacement control of vertical actuators (w=0 & θ_{top}=0): in addition to restraining the rotation at the wall top, the axial displacement is constrained too after having applied the normal force. This leads to a changing axial force throughout the loading process.
- Cantilever half the wall height (N=const.): the wall is modelled with only half of its actual height. The

horizontal excitation is applied at the new wall top; hence, cantilever boundary conditions for the half-height wall are achieved. The normal force N is again applied as point loads onto the rigid plate.

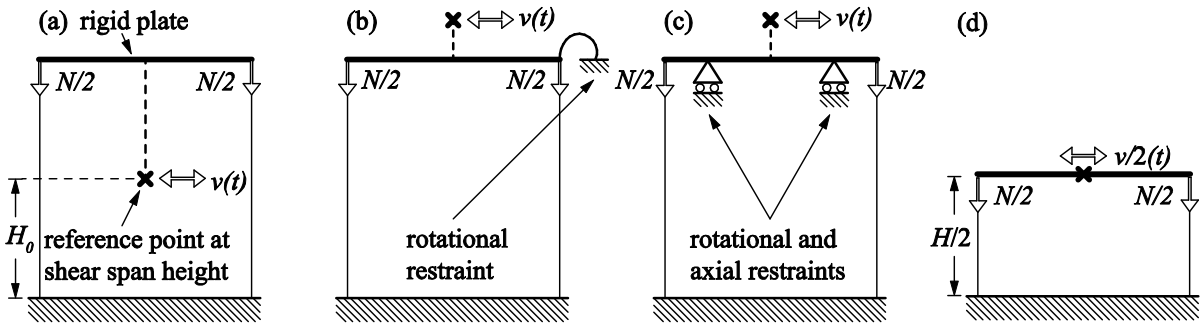

Figure 4: Different approaches to obtain fixed-fixed conditions in testing in numerical simulation, (a) keeping shear span constant, (b) restraining top rotation at zero, (c) restraining rotation and axial displacement on top, (d) testing cantilever with half the wall height

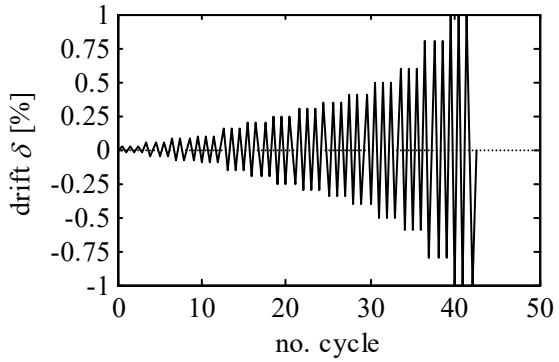

Figure 5: Loading protocol as used in the testing campaign by [6] shown up to a drift limit of 1%, applied to all the simulated walls

4 Results

The wall configurations described in Section 3.2 and Table 3 are analysed applying the cyclic loading protocol used by [6] that is shown in Figure 5. For each wall configuration, all four test setups that represent double-fixed conditions are simulated (Section 3.3) and the results compared in Figure 6-Figure 9. They present the envelopes of the shear force-drift response (a), the shear force-rotation (b) and the normal force-drift curves (c). The point of ultimate drift is defined as the point where the shear force in the post-peak drops for the first time below 0.8 times the peak shear force capacity and is indicated by a dashed line.

Figure 6a-Figure 9a show that the difference between force- and mixed-controlled modes in terms of shear force-drift curves is negligible. Theoretically they should be identical but the explicit numerical solution procedure leads to small differences. In reality, differences might also result from non-uniformly distributed

material properties within the wall panel and the gravity load due to the self-weight of the wall, which was neglected in the simulations. Differences are expected to be particularly evident in the post-peak response when damage localisation occurs. A difference between both approaches is a certain rotation of the wall top in the case of the force-controlled mode (as opposed to the mixed-controlled), which decreases with increasing axial load. This can be mostly attributed to the explicit numerical solution procedure in conjunction with the simulation of bed-joint sliding in the post-peak domain. As bed-joint sliding decreases with increasing axial load, the rotation at the wall top decreases too.

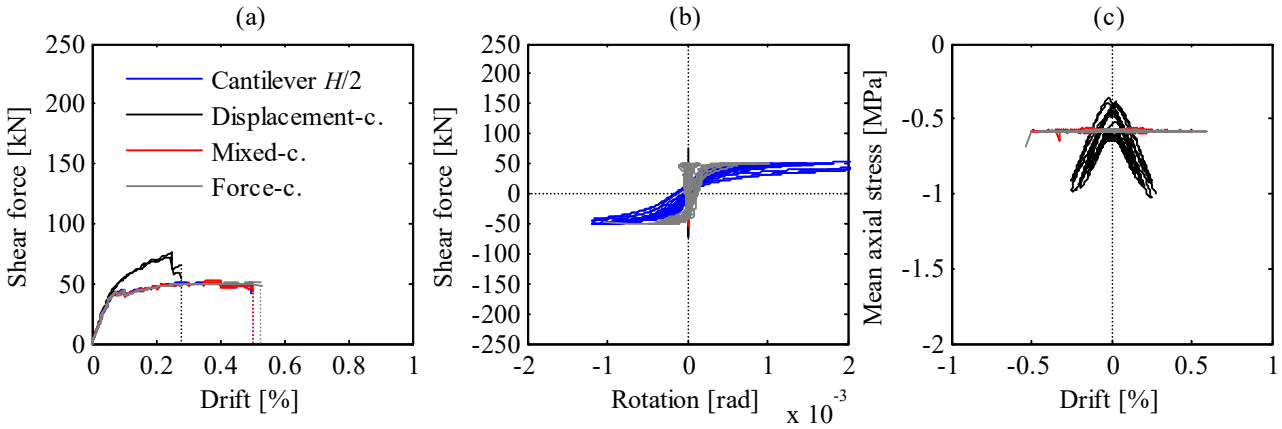

Figure 6: Wall T1 mod, (a) shear force-drift (envelop), (b) shear force-rotation and (c) mean axial stress-drift curve

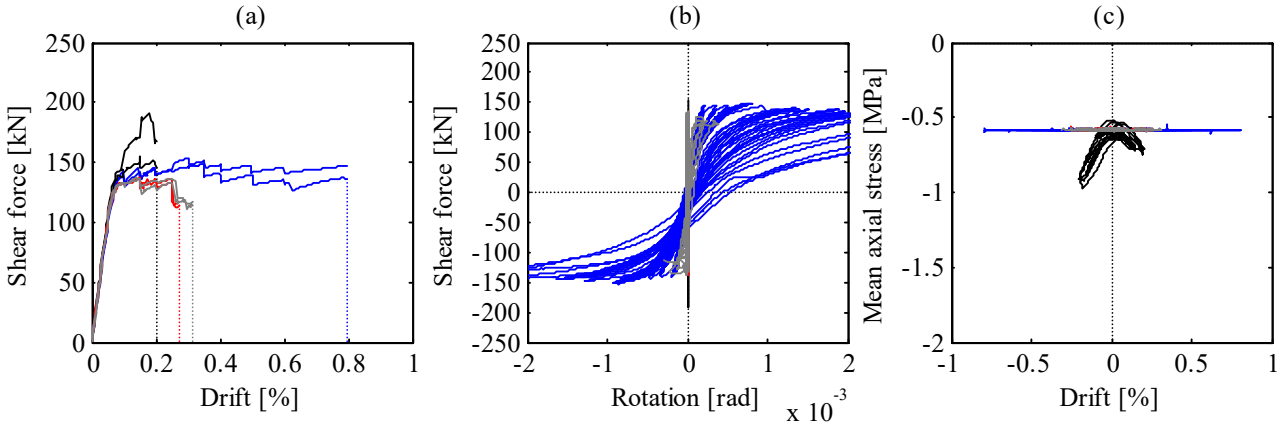

Figure 7: Wall T1, (a) shear force-drift (envelop), (b) shear force-rotation and (c) mean axial stress-drift curve

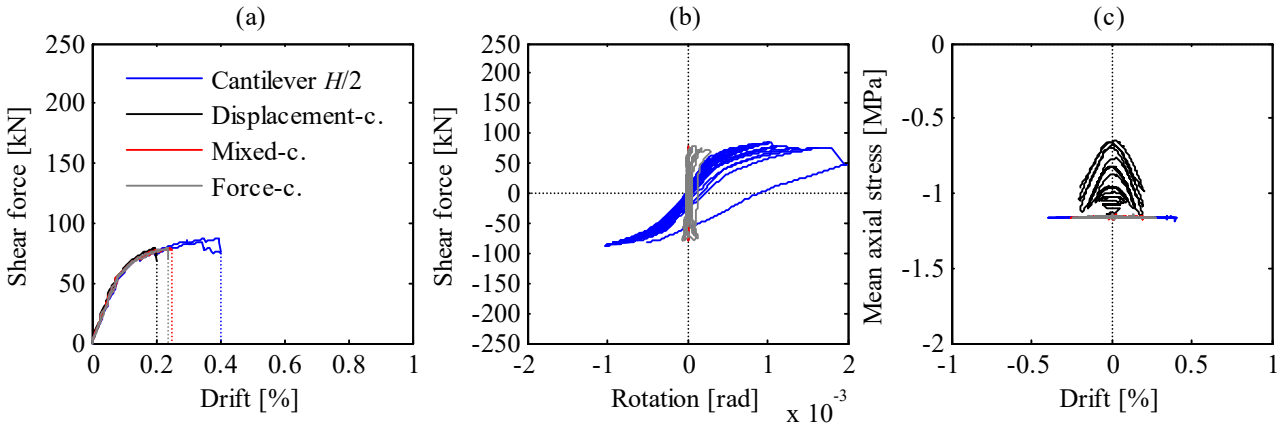

Figure 8: Wall T3 mod, (a) shear force-drift (envelop), (b) shear force-rotation and (c) mean axial stress-drift curve

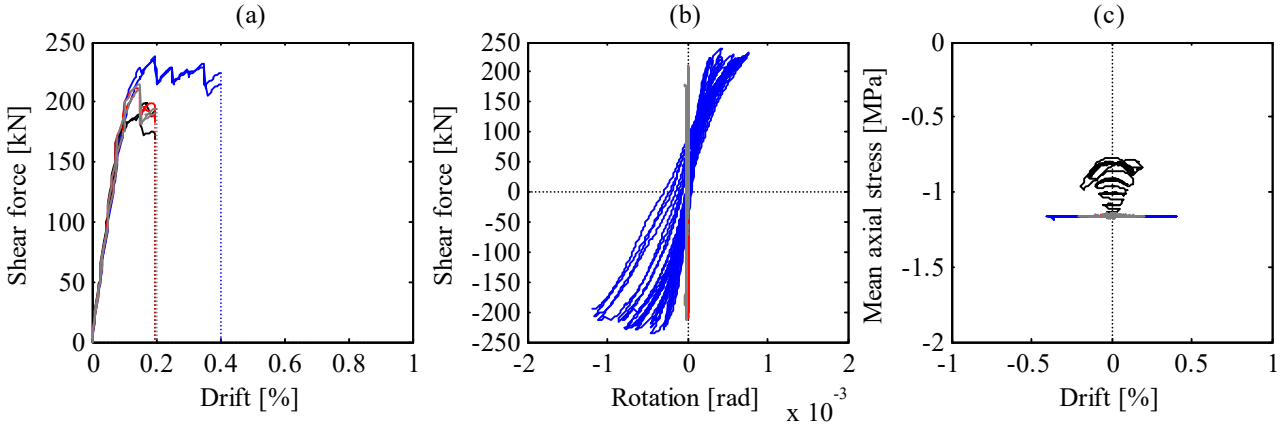

Figure 9: Wall T3, (a) shear force-drift (envelop), (b) shear force-rotation and (c) mean axial stress-drift curve

In the displacement-controlled mode, the vertical displacement is restrained after the axial load has been applied in the beginning of the test. This results in a change in normal force throughout the horizontal loading procedure. For walls that are subjected to a small initial axial load (see Figure 6 and Figure 7), the internal normal force increases with increasing drifts—small initial axial load means potentially more flexural uplift in the bed-joints (rocking), which would lead to an elongation of the wall if it were not vertically restrained. Therefore the internal normal force has to increase. This increase in normal force leads to a greater force capacity and a reduction in drift capacity due to more brick crushing compared to the other control modes. A reduction in drift capacity with increasing normal force has also been observed in multiple experimental programs, e.g. [1,4,6,7]. As for the case of a higher applied axial load (Figure 8 and Figure 9); in the beginning the internal normal force tends to decrease with increasing drifts and non-linearity of the force-displacement response as a shortening of the wall is prevented by the vertical restraint at the wall top. The drift capacity, however, is similar to the force- and mixed-controlled mode, as the internal normal force approaches the initially applied one towards the drift limits of the final cycles where potential shortening due to compressive

damage and potential elongation due to flexural uplift seem to cancel out each other's influences.

Testing a cantilever to simulate double-fixed conditions in a wall twice the height leads to an over-estimation of the drift capacities. Reasons for this are damage patterns that do not correspond to 'real' damage under double-fixed conditions (i.e. diagonal cracking with crushed zones in the center of the wall where the two cracks meet, see Figure 10) and a higher ratio of confined to un-confined wall area. With regard to the force capacities, this approach appears to yield similar results as the force- and mixed-controlled mode for the case of lower axial loads while it over-estimates them for higher axial loading.

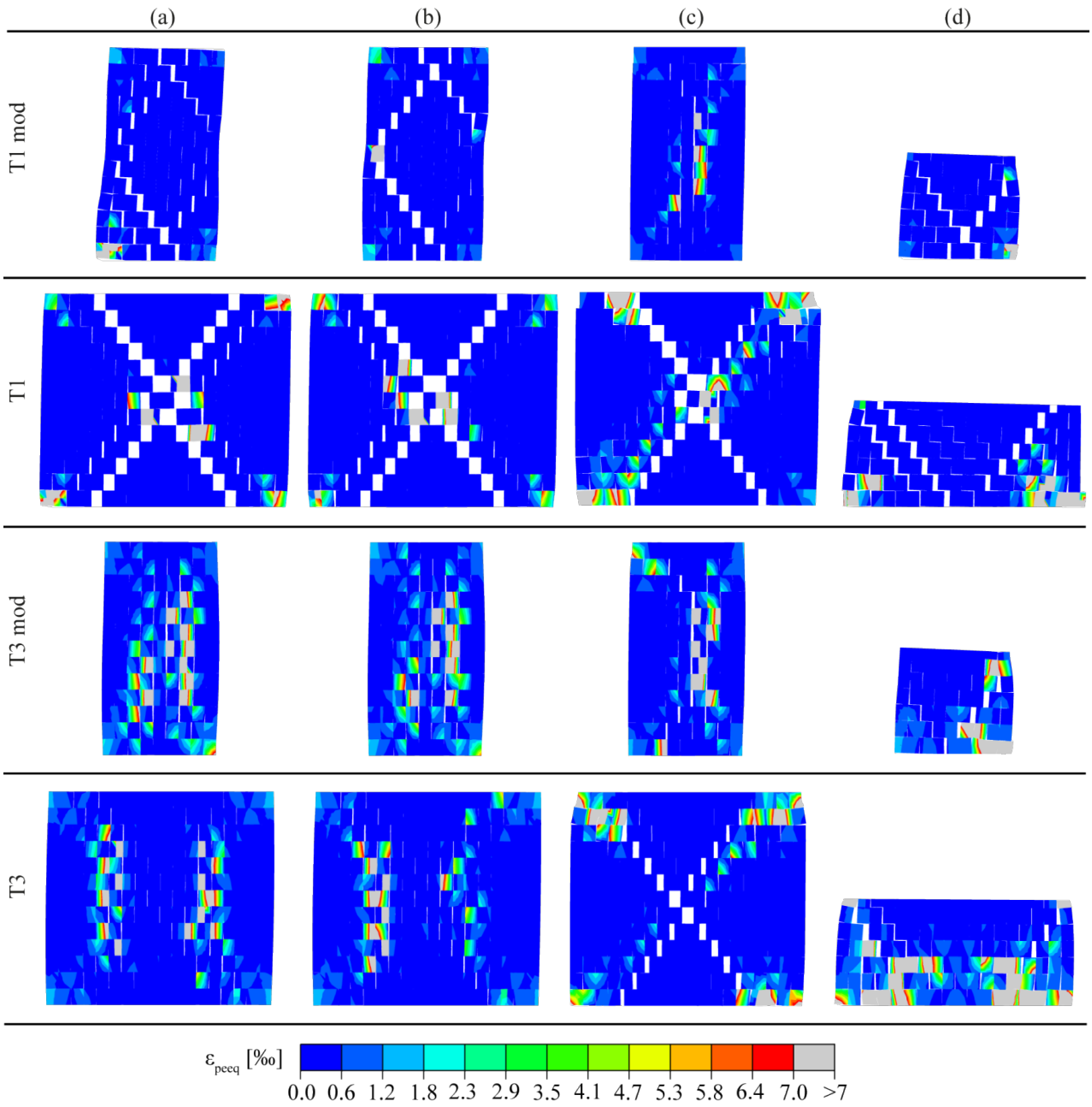

Figure 10: Deformed shape (magnification factor of 10) including plots of equivalent plastic strains in the solid elements of simulated walls around ultimate drift: (a) force control, (b) mixed control, (c) displacement control, (d) cantilever of

half the wall height

Figure 10 shows the deformed shapes magnified by a factor of ten of all the simulated walls at ultimate drift. Included in those figures are plots of the equivalent plastic strains (ε_{peeq}) in the solid elements. Within the 'Concrete Damaged Plasticity' model in Abaqus [18], equivalent plastic strains (ε_{peeq}) are a scalar measure, computed from the plastic strain components, of how far the current stress-strain state in the element has progressed along the assigned in-elastic uni-axial stress-strain law in compression. It can therefore be seen as a good representation of brick crushing.

The deformed shapes agree with the above-mentioned differences in force-displacement response according to the used control mode. It is particularly evident for the difference between the cantilever approach and the other control modes. In all the cases where the drift capacity for the cantilever approach is significantly higher than for the other modes (i.e. walls T1, T3 mod and T3), the damage patterns between the respective walls are very different with respect to the direction of diagonal cracking and the amount of crushing within the wall. Only for wall T1 mod, where the drift capacities are comparable among force, mixed control and cantilever approach (see also Figure 6a), the damage patterns match.

The difference in damage patterns between force and mixed control is quite small, which also explains the very similar performances of both control modes in terms of force-displacement response, force and drift capacity.

With regard to the difference between displacement-controlled mode and force or mixed control, there is clearly more crushing within the displacement-controlled wall panel for walls with a lower axial pre-compression (i.e. wall T1 mod and T1). This is reflected in the lower drift capacity of the displacement-controlled wall with respect to force and mixed control in these cases, see Figure 6a and Figure 7a. For higher pre-compression, the amount of crushing is comparable among the modes (force, mixed and displacement) for wall T3 mod while the damage pattern for T3 shows more bed-joint sliding in the displacement-controlled case due to the decrease in internal normal force in the course of horizontal loading and finally more toe crushing as the internal normal force increases again towards the final displacement cycles. Both results in similar drift capacities among force-, mixed- and displacement controlled mode.

5 Conclusions

This article treats the influence of test setups that simulate fixed-fixed boundary conditions on the force and drift capacities of in-plane loaded URM walls by means of a numerical study. At the base, the walls are always supported by a stiff foundation. At the wall top, the three in-plane degrees of freedom are controlled in various ways. Four principally different test setups have been reported in the literature. The first three have in common that the horizontal displacement is applied at the top of the wall according to a chosen loading protocol. However they differ concerning the control of the vertical and the rotational degree of freedom, which can either be treated as static or kinematic quantity. The three modes of control can therefore be described as force control, mixed control and displacement control. In the fourth experimental setup, a specimen half the wall height is tested as a cantilever and subjected to a constant axial load.

It shows that both force- and mixed-controlled setups lead to nearly completely equivalent results concerning the shear-force drift behaviour of URM walls while the displacement-controlled mode leads to a change in axial loads. This results in lower drift capacities and higher shear force capacities for low axial load ratios but lower force capacities and comparable drift capacities for higher axial load ratios. The approach of testing a cantilever to simulate a wall under fixed-fixed conditions with twice the height results in a significant over-estimation of the displacement capacity since the damage pattern does not correspond to those observed for the other control modes due to the confining effect of the loading beam.

While the approach of testing a specimen of half the wall height does not yield results that are representative of a wall that is subjected to double-fixed conditions, the choice between a force-controlled, mixed-controlled or displacement-controlled mode depends on which real boundary conditions are to be simulated. If the axial extension is mechanically restrained, the displacement-controlled mode might be most appropriate. In many cases however it may be assumed that the axial force in an unreinforced masonry wall depends largely on the gravity load and remains approximately constant; in this case the force-controlled or the mixed-controlled mode would be more accurate. The choice between one and the other depends here mainly on capabilities of the test setup and preferences of the researcher. In buildings with masonry spandrels or reinforced concrete ring beams or slabs, the axial load in the wall may vary due to the shear force transferred by spandrel, beam or slab. Such a configuration was simulated in the last test reported in [11]. At present, the influence of a varying axial force on the drift capacity of an unreinforced masonry is not yet known and further experimental and

numerical research on the influence of a variable axial force is needed.

It shall further be emphasized that a numerical study cannot be seen as fully representative of reality. It is supposed to be a complementary part that gives some insight into the influence of different testing approaches for fixed-fixed boundary conditions on the wall capacity describing parameters which should be validated by an experimental study.

6 Acknowledgement

This study has been supported by the grant no. 159882 of the Swiss National Science Foundation: “A drift capacity model for unreinforced masonry walls failing in shear”.

7 References

[1] Ganz H, Thürlimann B. Versuche an Mauerwerksscheiben unter Normalkraft und Querkraft. Test Report, ETH Zürich: 1984.

[2] Magenes G, Calvi GM. Cyclic behaviour of brick masonry walls. Earthq Eng Tenth World Conf Rotterdam 1992.

[3] Bosiljkov V, Tomaževič M, Lutman M. Optimization of shape of masonry units and technology of construction for earthquake resistant masonry buildings - Part One and Two. Lubljana, Slowenia: 2004.

[4] Bosiljkov V, Tomaževič M, Lutman M. Optimization of shape of masonry units and technology of construction for earthquake resistant masonry buildings - Part Three. Lubljana, Slovenia: 2006.

[5] Magenes G, Morandi P, Penna A. D 7.1c Test results on the behaviour of masonry under static cyclic in plane lateral loads. Pavia: 2008.

[6] Salmanpour AH, Mojsilović N, Schwartz J. Displacement capacity of contemporary unreinforced masonry walls: An experimental study. Eng Struct 2015;89:1–16. doi:10.1016/j.engstruct.2015.01.052.

[7] Petry S, Beyer K. Cyclic Test Data of Six Unreinforced Masonry Walls with Different Boundary Conditions. Earthq Spectra 2015;31:2459–84. doi:10.1193/101513EQS269.

[8] Graziotti F. Experimental campaign on a clay URM full-scale specimen representative of the Groningen building stock. Pavia, Italy: 2016.

[9] Graziotti F, Rossi A, Mandirola M, Penna A, Magenes G. Experimental characterisation of calcium-silicate brick masonry for seismic assessment. Proc 16th Int Brick Block Mason Conf 2016:1619–27.

[10] Messali F, Ravenshorst G, Esposito R, Rots J. Large-scale testing program for the seismic characterization of Dutch masonry walls. 16WCEE Santiago Chile 2017.

[11] Petry S, Beyer K. Influence of boundary conditions and size effect on the drift capacity of URM walls. Eng Struct 2014;65:76–88. doi:10.1016/j.engstruct.2014.01.048.

[12] Wilding BV, Dolatshahi KM, Beyer K. Influence of load history on the force-displacement response of in-plane loaded unreinforced masonry walls. Eng Struct 2017;152:671–82. doi:10.1016/j.engstruct.2017.09.038.

[13] Aref AJ, Dolatshahi KM. A three-dimensional cyclic meso-scale numerical procedure for simulation of unreinforced masonry structures. Comput Struct 2013;120:9–23. doi:10.1016/j.compstruc.2013.01.012.

[14] ATC. FEMA 461: Interim Testing Protocols for Determining the Seismic Performance Characteristics of Structural and Nonstructural Components. Applied Technology Council (ATC), Washington DC,

2007.

[15] Petry S, Beyer K. Scaling unreinforced masonry for reduced-scale seismic testing. Bull Earthq Eng 2014;12:2557–81. doi:10.1007/s10518-014-9605-1.

[16] Tomaževič M. Some aspects of experimental testing of seismic behavior of masonry walls and models of masonry buildings. ISET J Earthq Technol 2000;37:101–17.

[17] Salmanpour AH, Mojsilovic N. Simulation of boundary conditions for testing of masonry shear walls. AIP Conf Proc 2015;1702:1–5. doi:10.1063/1.4938935.

[18] Dassault Systèmes. Abaqus 6.14 Documentation. Providence, RI, USA: Dassault Systèmes Simulia Corp.; 2014.

[19] Lourenço PB. Computational strategies for masonry structures. PhD-Thesis, TU Delft, 1996. doi:ISBN 90-407-1221-2.

[20] Oliveira D V., Lourenço PB, Roca P. Cyclic behaviour of stone and brick masonry under uniaxial compressive loading. Mater Struct 2007;39:247–57. doi:10.1617/s11527-005-9050-3.

[21] Kaushik HB, Rai DC, Jain SK. Stress-Strain Characteristics of Clay Brick Masonry under Uniaxial Compression. J Mater Civ Eng 2007;19:728–39. doi:10.1061/(ASCE)0899-1561(2007)19:9(728).

[22] Gopalaratnam VS, Shah SP. Softening Response of Plain Concrete in Direct Tension. ACI J 1985;82:310–23. doi:10.14359/10338.

[23] Dolatshahi KM, Nikoukalam M, Beyer K. Numerical study on factors that influence the in-plane drift capacity of unreinforced masonry walls. Earthq Eng Struct Dyn 2017;submitted.